APEM journal
Advances in Production Engineering & Management
Volume 14 | Number 1 | March 2019 | pp 15–26
https://doi.org/10.14743/apem2019.1.308
ISSN 1854-6250
Journal home: apem-journal.org
Original scientific paper

Determination of nano-roughness for micro-objects by measuring the van der Waals force

Bratina, B.[a,*], **Šafarič, J.**[a], **Uran, S.**[a], **Šafarič, R.**[a]

[a]Faculty of Electrical Engineering and Computer Science, University of Maribor, Maribor, Slovenia

ABSTRACT

3D printing or assembly techniques in the micro/nano-world enable production of micro-parts for building small machines or structures for biomedicine applications, such as cultivation of living cells in the field of Tissue Engineering. Micro-sized assembly requires automated manipulation procedures and methods for determination of suitable objects for assembly. The latter is possible by van der Waals force measurement and determination of distance at the van der Waals peak between two objects in contact. They are dependent not only on the Hamaker coefficients of the materials in contact and their geometries, but also on the nano-roughness asperities and crystal structure asperities of the contact surfaces. A method is presented for measuring van der Waals` force and determining micro-objects' (sizes between 10-100 μm) distances between materials in contact at the van der Waals peak in the presence of nano-roughness and crystal structure roughness. The proposed model was validated by experimental lab results between various materials and shapes (glass and polystyrene beads, metallic wires).

ARTICLE INFO

Keywords:
Micro-object;
Surface roughness;
Nano-roughness;
Van der Waals force;
Distance at van der Waals peak

**Corresponding author:*
bozidar.bratina@um.si
(Bratina, B.)

Article history:
Received 14 September 2018
Revised 18 February 2019
Accepted 24 February 2019

1. Introduction

3D printing is becoming an essential part of rapid prototyping in Research and Development Departments. Today, classic and novel printing technologies enable printing of almost everything that can be designed. Also, the variety of printing materials and composites is increasing on the market (plastics, imitation wood, metals, etc.), which also makes possible prototyping of high end industrial products (jet engine blades, high-temperature and high-pressure rocket engine combustion chambers [1], airplane parts, etc.). However, additive manufacturing on a small scale, such as micro/ nano level 3D printing, presents one of the challenges. Scientists have developed many different deposition and hardening techniques (electron beam lithography, multiphoton polymerization, etc.), which enable printing of small objects to a micron level [2]. These 3D printing technologies have in common operating with light sensitive materials, resins, powders as an additive material which can later be treated for hardening. On the other hand, 3D printing can also be managed by using micro/nano-objects assembled into a microstructure layer by layer [3, 4] (micro-machines, gearbox, motor, etc.), or structures with living cells, which could boost the field of Tissue Engineering.

To be able to assemble given micro-objects into a structure, it is essential to have adequate equipment and to master the manipulation of material. Automated assembly procedures with micro/nano-manipulators include sensors to control the assembly process, hence detecting micro-objects for assembly, which are too small for machine vision applications. Therefore, a

method is needed to be able to determine if the object for assembly is adequate or not (dust particle, micro-object not adequate in size or material). In the paper such a method is presented, where micro-object' properties are measured by van der Waals force, and distances at van der Waals peak are determined between materials in contact. Similar measuring methods (atomic force microscope measurements, X-ray method etc.), are performed very rarely due to the expensive equipment used, whereas the presented method is quite simple, and gives similar accuracy results.

Van der Waals force and distance at van der Waals peak

Even on fine polished solid surfaces of materials (glass or polystyrene microbeads, metal wires, etc.), asperities are large in comparison with the size of the crystal structure (atoms or molecules) of the solid materials placed in contact. Most materials used in engineering practice have surface asperities (so-called nano-roughness) greater than few decades of a nano-metre. If two such solid materials are placed in contact, because of the mentioned asperities, the great areas of surfaces will be separated by a distance much greater than the molecular range of action [5]. Previously developed models of van der Waals forces [3] for a one-finger gripper, based on the van der Waals force, demand an accurate calculation of the van der Waals force at the point of contact. The van der Waals force between two objects in contact is dependent on the geometry of the objects, their materials (Hamaker coefficients), and the distance between the objects in contact. This paper focuses on the determination of the distances between objects in contact, with the presence of nano-roughness asperities and crystal structure asperities on both the contact surfaces (distance at van der Waals peak, Fig. 1). An assembly application of micro structures from micro/nano-objects [3] demands characterization of material properties, the identification and manipulation of micro-objects, and assembly techniques. For identification of the geometric features of a micro-sized object (size, diameter in the case of spherical or cylindrical shapes …), measurements of the van der Waals contact forces are necessary, and demand an accurate measurement of the surface roughness of the micro-object. Determining the surface roughness of a micro-object has been proven to be problematic, whereas present methods can only give an inaccurate estimation or calculation of the roughness and, consequently, the van der Waals contact force. Three methods exist for measuring or determining the roughness of micro-sized objects.

The first one, originally described by Rowland and Taylor [6], and later used by Alvarez [7], calculates the distances at van der Waals peak statistically from the distribution of intermolecular distances (Fig. 1) between most of the elements in the periodic system against a so-called oxygen probe. This method is based on the statistical analysis of the intermolecular contacts in X-ray crystal structures for determining the van der Waals radii. However, with this method, only the distances at van der Waals peak between the periodic system elements and the oxygen probe have been determined and published, while the contacts for a variety of other materials (except sulphur and hydrogen probes) have not yet been studied to the knowledge of the authors of this paper. The second method is the so-called analytical method, first described in Rumpf [8], and later used as a modified version by various authors [9-12, 14]. For this method, the square root of the mean square values of the surface roughness is measured with a precise AFM (Atomic Force Microscope), or by the electron beam evaporation method. The different models based on this method assume that the asperities are hemispherical caps on a smooth substrate [8]. Matope *et al*. [13] have suggested that the adhesion (van der Waals) force on surfaces exhibiting asperities should be written as a combination of sphere–sphere and sphere–plane surface interactions in the form:

$$F_{adh} = \frac{A\,R}{6\,H_0^2}\left(\frac{1}{1+58\,R\,rms/\lambda^2}+\frac{1}{(1+1.82\,rms/H_0)^2}\right) \quad (1)$$

where A is the Hamaker coefficient, R is the radius of the micro-sized spherical object, H_0 is the contact distance between the surface and the object, *rms* is the root of mean square values of the micro-object's surface roughness, and λ is the peak-to-peak distance of the asperities of the surface roughness of the micro-object. These models calculate the van der Waals force between

various micro-sized objects (spheres or blunt particles), where the *rms* of the surface roughness is measured on only one side of the materials in contact (usually the plane surface), while the *rms* of the surface roughness of the probe (sphere) is not measured at all.

Instead, the distance $H_0 = 2\text{-}3$ Å ($1\text{Å} = 10^{-10}$ m) is used between the material and the probe (sphere). The drawback of this model is that it gives precise results only for F_{adh}, where the probe has the exact value inside $H_0 = 2\text{-}3$ Å. Moreover, the difference between F_{adh} for the case when $H_0 = 2$ Å or 3 Å, is more than 40 %. So, this method is quite inaccurate. Of course, this model is only suitable for calculating the van der Waals force between a plane surface and a sphere particle. The third method is the so-called computational method, which is in good agreement with our experiments [14]. The drawback of the third method is its complexity (fractal surfaces, Fourier Transforms), which makes it hard to apply, especially for quick estimations of the van der Waals force for specific systems.

Our presented method solves all mentioned drawbacks (distances at van der Waals peak are known only for the elements of the periodic system against an O-probe, the use of only one side of a surface in contact, the distance $H_0 = 2\text{-}3$ Å produces huge errors in order to calculate the van der Waals force, and the complexity of the Eichenlaub's method). The developed method for determining the distance at van der Waals peak in the presence of nano-roughness and the crystal structure roughness of contact surfaces, is valid for arbitrary materials (not only pure elements against an oxygen probe) of micro-sized objects. In addition, it is also suitable for situations where two objects with different geometries have their own surface roughness. The developed surface model can also determine the roughness of the materials' surfaces in contact (distances at van der Waals peak) between micro-objects with materials 1 and 2, if the previously determined roughness between micro-objects with materials 1 and 1 and materials 2 and 2 are known. Moreover, it is simple to use, because its equations rely on only one parameter (distance at van der Waals peak), which is determined easily from the van der Waals force measurements. It is not necessary to use an AFM, beam-electron or other expensive microscopes.

The paper structure is as follows. The second section of the paper presents a description of the method for determining distances at van der Waals peak in the presence of nano-roughness and crystal structure roughness on contact surfaces. The next section describes the laboratory set-up and the set of used equations for calculating the van der Waals force of two micro-sized objects in contact with different geometries, different materials and different roughness of materials. The third section presents experimental results and analysis, and fourth the conclusion of the paper.

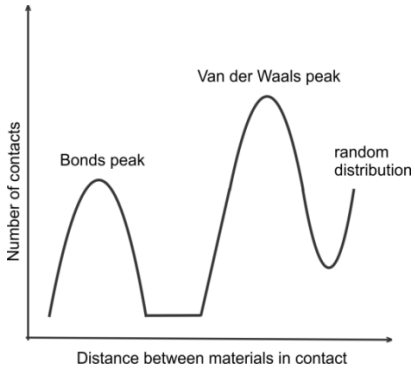

Fig. 1 Scheme for determining the distance between materials in contact at van der Waals peak

2. Materials and methods for surface roughness determination (distance at van der Waals peak)

The determination of the distance at van der Waals peak demands precise measurements of the van der Waals force between two objects in contact. We focused on micro-sized objects of different shapes: Plane surface, cylinder with a radius of 25 μm, and spheres with a radius of 5-50 μm, chosen because of their availability on the market, which gives us the following van der Waals

force measurement pairs: Plane surface-sphere, sphere-sphere, sphere-cylinder and cylinder-cylinder. The other two possible types of measurements, plane surface-plane surface and cylinder-plane surface, are not practical, due to problems with the alignment of both objects. Therefore, our method is based on four practical geometrical pairs. The laboratory set-up hardware was designed for 3D movement of both objects against each other.

2.1 Laboratory set-up and materials used in the experiments

The laboratory set-up is shown in Fig. 2a. The nano-precision 3D manipulator system consists of an optic microscope, a turbo-molecular vacuum pump and a vacuum chamber with nano-precision 3D manipulator (Fig. 2b) inside. The vacuum can be set as low as 2 μbar. Fig. 2b shows the nano-precision 3D manipulator mechanism, with x- and y-axes consisting of magnetic linear incremental encoder sensors that operate as a planar mechanism, and a z-axis with its own linear incremental sensor. Different end-effectors (tools, grippers, etc.) can be mounted on the 3D manipulator tip at the end of the y-axis. The y-axis is placed on a movable cart that moves along the x-axis' linear guide. All three piezo electric motors with sensors are mounted on an aluminium block that serves as a vibration-absorber to limit mechanical disturbances from the environment. The position accuracy of the robotic tip, along a single axis, is ± 3.9 nm in an open loop, while the position control loop of each axis has an accuracy of ± 61 nm. We also used a long distance focus (21 mm) optical microscope for observations of micro-objects up to 3 μm. A more precise description of the lab set-up can be found in [3, 4, 15].

Different micro-sized objects were used in the experiments: Metal wires, glass (SiO_2) and polystyrene beads, glass surfaces and mica surfaces. The glass beads (radius 25-50 μm and 10-30 μm) were purchased from Polysciences, Inc., USA. The polystyrene beads (radius of 30 μm) were purchased from Kisker Biotech GMBH, Germany. The nickel wire (puratronic, radius 25 μm, LOT: E22Z008), palladium wire (hard, radius 25 μm, LOT: L15T030), aluminium wire (hard, radius 25 μm, LOT: G24Z014), silver wire (Premion, radius 25 μm, LOT: 13467) and gold wire (Premion, radius 25 μm, LOT: P21A023) were purchased from Alfa Aesar GmbH, Germany. All the metal wires had 99.99 % trace metals basis. Standard microscope slides (SiO_2) were used for the glass surface plane, purchased from Logitech, UK. The Muscovite mica insulating slides were purchased from EA Elektronika, Slovenia.

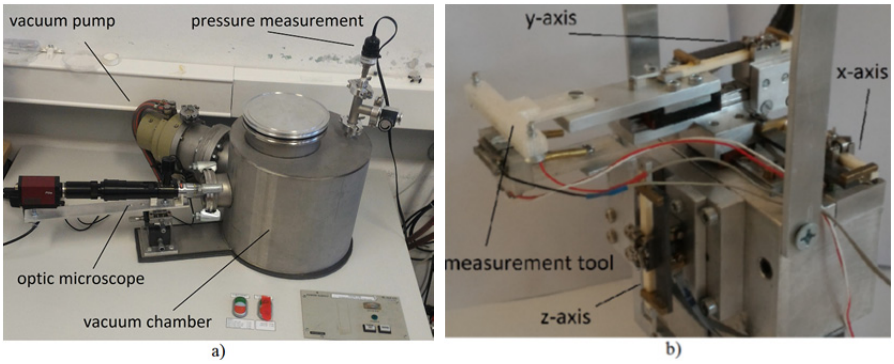

Fig. 2 The nano-precision 3D manipulator system a), and the nano-precision 3D manipulator mechanism b)

2.2 Used methods: Pull-off measurements of the van der Waals force

Small attraction forces, such as the van der Waals forces between micro-sized objects in contact, are often measured using an AFM microscope. However, the presented pull-off method consisted of measuring the attraction force using a spring traverse [16]. Fig. 3 shows a schematic diagram of the four different types of measurements of the van der Waals forces between the geometrically different objects used in our experiments. The attraction force F_{ATR} attracts the micro-sized objects when they have been put into contact. If the lower object is pulled away by the force F with z-axis (Fig. 3), then the traverse starts to deflect with the distance f. The objects are "attached" together during the deflection due to the attraction force, and the objects in contact keep this position until the opposite traverse's elastic force F becomes equal to the attraction force. At that moment, the traverse tears away from the lower object towards a position of equilibrium,

hence, the deflection f is measured. Calculation of the traverse's deflection force F and inertia I_z [17] for a circular cross-section is presented by Eq. 2:

$$F = \frac{3fEI_z}{l_T^3}, \quad I_z = \frac{\pi d^4}{64} \quad \Rightarrow \quad F_{ATR} = F = \frac{3fE\pi d^4}{l_T^3 64} \tag{2}$$

where l_T is the length of the traverse, E is its Young's modulus, and d is its diameter. The measurements of F_{ATR} were conducted in a vacuum chamber with pressure lower than 1 mbar to avoid capillary force effects. The static electric charge on the SiO_2 (amorphous) plane surface was discharged by putting the tip of the traverse into contact with the plane surface for a moment, thus equalising the electrical charges. Both the traverse and the plane were also grounded electrically. Consequently, the capillary and electrostatic forces were avoided.

Fig. 4a shows the measurement tool on the robotic tip with a mounted golden traverse and a glass plane, where the spherical object is glued. Fig. 4b shows the golden traverse touching the spherical glass object. The traverse and the object in Fig. 4b were observed through a microscope (the diameter of the traverse is 50 μm).

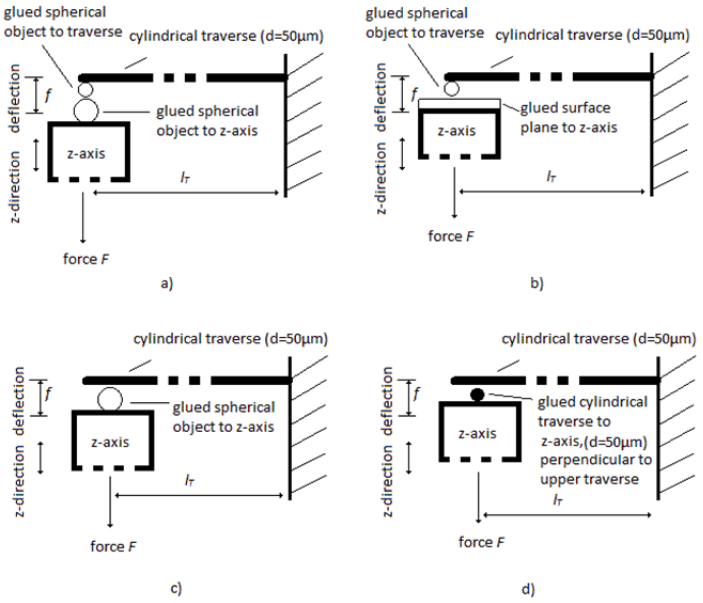

Fig. 3 Schematic diagram of the four methods used for measuring attraction forces: a) Between micro-sized spheres, b) Between micro-sized spheres and the surface plane, c) Between micro-sized spheres and a cylinder and d) Between two perpendicular cylinders

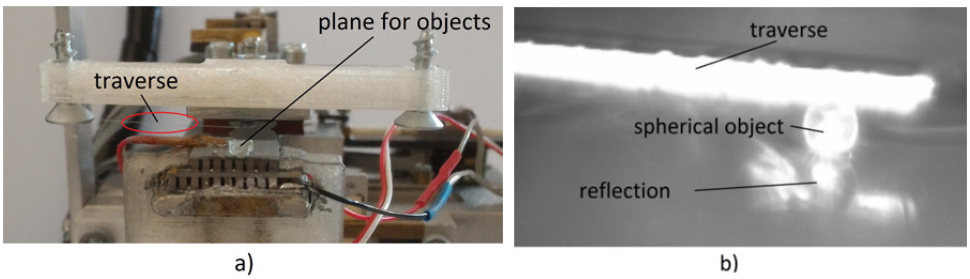

Fig. 4 Measurement tool a), and zoomed view - traverse touching a spherical object b)

2.3 Proposed model for determining the distance at van der Waals peak

Four models were developed for determining (calculating) the distance at van der Waals peak from the measured van der Waals force $F = F_{ATR}$ (Eq. 2) which are presented next. The models for determining the distance at van der Waals peak for the following examples: Sphere-sphere (Fig. 3a), sphere-surface plane (Fig. 3b), and between two perpendicular cylinders (Fig. 3d) are easy to develop from known analytical equations for the van der Waals force between different

geometrical objects [18-20]. The equations used for determining the average contact distance d or the distance at van der Waals peak are as follows:

a) For sphere - sphere geometrical combination:

$$F = \frac{AR_1R_2}{(R_1+R_2)6d^2} \quad \Rightarrow \quad d = \sqrt{\frac{AR_1R_2}{(R_1+R_2)6F}} \tag{3}$$

b) For sphere - surface plane there is an approximate formula:

$$F = \frac{AR}{6d^2} \quad \Rightarrow \quad d = \sqrt{\frac{AR}{6F}} \tag{4}$$

c) And for two infinite perpendicular cylinders of the same radius, there is again an approximate formula:

$$F = \frac{AR_c}{6d^2} \quad \Rightarrow \quad d = \sqrt{\frac{AR_c}{6F}} \tag{5}$$

where A is the Hamaker coefficient, R_1, R_2, R are the radii of the spheres, R_c is the radius of the cylinder, and F is the van der Waals force in contact (F_{ATR}), measured and calculated by Eq. 2. The situation is far more complex in the case when the distance at van der Waals peak is determined between a cylinder and a sphere. We found two sources [19, 21] where the authors claimed that they had developed an analytical expression for the van der Waals force between a sphere and an infinitive cylinder. Unfortunately, the expression used by Montgomery [19] was proven experimentally to be incorrect, due to an imprecise use of the Maclaurin series. Ref. [21] showed promising results when the expression was verified experimentally for the van der Waals force in contact. We have tried, unsuccessfully, to repeat the analytical development of the final result of ref. [21]`s complicated expression, which is written as:

$$F = \frac{AR_s^3\left\{(4+2s+s^2)E\left(\frac{1}{p}\right) - s(1+s)K\left(\frac{1}{p}\right)\right\}}{24c^{5/2}R_c^{3/2}s^2p^{3/2}} \tag{6}$$

where $p = 1+ s/2$, $s = ((d + R_s)^2 - R_s^2)/(2cR_c)$, $c = R_c + R_s + d$, d is the distance between the sphere and the cylinder, R_c is the radius of the cylinder, R_s is the radius of the sphere, K and E are the complete elliptic integrals defined as:

$$E(z) = \int_0^{\pi/2} \sqrt{1 - zsin^2\theta}\, d\theta, \tag{7}$$

$$K(z) = \int_0^{\pi/2} 1/\sqrt{1 - zsin^2\theta}\, d\theta. \tag{8}$$

Instead of Eq. 6 [21] we derived our equation (9) for van der Waals force calculation between an infinite cylinder and a sphere from the same mathematical and physical assumptions. Both Eq. 6 and Eq. 9 were compared between themselves. We can confirm that the original equation derived in [21] is correct, because both equations gave the same numerical results for F when the distance d was used between 0.2 nm to 200 nm. Unfortunately, both Eq. 6 and Eq. 9 are not completely analytical, because it is not possible to derive analytical equations from them for the distance d.

$$F = AR_s^3 \int_{R_s+d}^{R_s+R_c+d} \frac{r(c^2 - r^2 + R_c^2)}{c(-r^2 + (c-R_c)^2)^{1/2}(r^2 - (c+R_c)^2)^{1/2}(r^2 - R_s^2)^{5/2}}\, dr \tag{9}$$

Both equations demand numerical calculation of the complete elliptic integrals or finite integrals. In order to calculate the distance d from the van der Waals force F, the theory of Artificial Neural Network was used to approximate the nonlinear inverse function of Eq. 6 and Eq. 9. The

classical backpropagation learning rule was used for a two-layer feedforward neural network, with one input, one output, ten neurons in a hidden layer, and one neuron in the output layer of the network. The learned Artificial Neural Network serves as a nonlinear calculator for the distance d (distance at van der Waals peak) between a sphere and an infinitive cylinder when the measured van der Waals force F is used, (see Fig. 3c) [22]. The tolerance, between the approximated and reference value of distance at van der Waals peak, after the Artificial Neural Network learning phase (150 iterations), was lower than 0.1 % for all the reference values of distance at van der Waals peak between 0.1 nm to 200 nm. The learning input samples (training vector) consisted of 100 pairs of distance at van der Waals peak and their corresponding values of the van der Waals force F. The Artificial Neural Network was learned in only 100 samples of the training vector. The approximated values of distance at van der Waals peak were also valid and accurate between the mentioned learning points, due to the generalization between data pairs.

2.4 Determining the distance at van der Waals peak when both interacting objects have roughness

The experiments published in [9-12] studied the nano-roughness, distribution of nano-roughness asperities and contact distances in the case where the measurement of an SiO_2 spherical probe roughness was not known, but assumed to be between 2-3 Å. Our newly proposed method takes into account both contact surfaces and their roughness affected by nano-roughness asperities and the crystal structure roughness of the contact surfaces – mentioned as the distance at van der Waals peak. Fig. 5 shows the scheme for describing contact surfaces with nano-roughness asperities and asperities due to the crystal structure of the material. The scheme in Fig. 5a shows the distance at van der Waals peak due to roughness d_{11} between two objects of material 1. Fig. 5b shows the distance at van der Waals peak due to the roughness d_{22} between two objects of material 2, while Fig. 5c presents the distance at van der Waals peak due to the roughness d_{12} between two objects of both materials 1 and 2.

The following equation can be stated hypothetically:

$$d_{12} = \frac{d_{11}}{2} + \frac{d_{22}}{2} \Rightarrow d_{11} = 2d_{12} - d_{22} \Rightarrow d_{22} = 2d_{12} - d_{11}. \tag{10}$$

So, if we can determine distances d_{11} and d_{22}, then we can determine the distance d_{12}, or vice versa. Therefore, if two distances at van der Waals peak are determined, it is possible to calculate a third one. In the following section, the experimental laboratory measurements are presented, proving Eq. 10 and the models for calculating the van der Waals force in contact, described by Eq. 3, Eq. 4, Eq. 5 and Eq. 9.

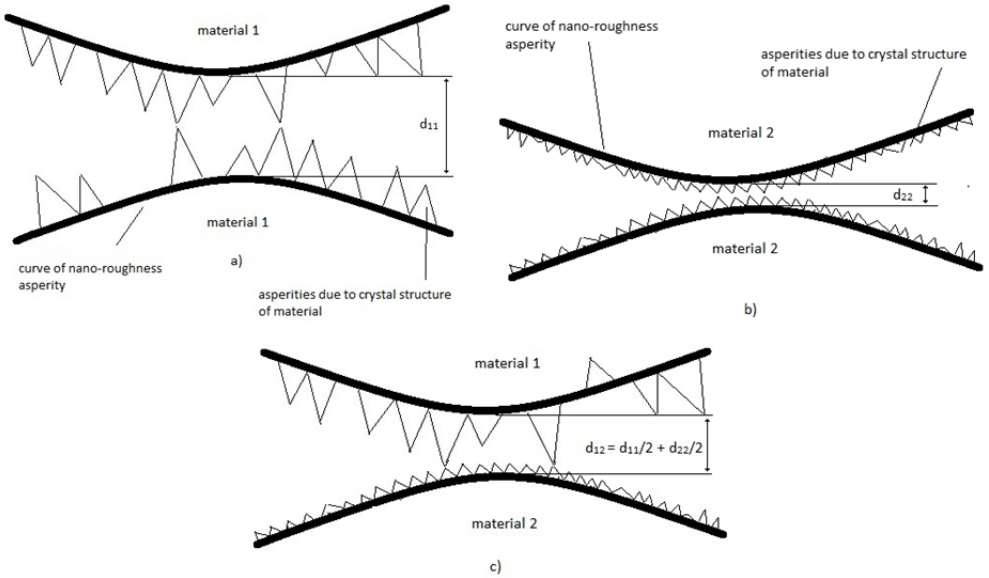

Fig. 5 The scheme of a cross-section of the distance at van der Waals peak due to nano-roughness asperities and the crystal structure asperities of the material in contact

3. Results and discussion

Three different geometries and several different materials of micro-objects were used in the experiments, as described in subsections 2.2 and 2.3: Au cylinder, Ag cylinder, Al cylinder, Ni cylinder, Pd cylinder, polystyrene sphere, SiO_2 sphere, SiO_2 plane and a mica plane.

3.1 Measurements

Thirty-two sets of measurements were done between different combinations of materials and geometries. Every set of measurements was done with twenty repetitions of measurements of deflection *f*. After that, the measurements were eliminated which departed heavily from the average (1-6 measurements out of 20).

The measured van der Waals force F_m (see Eq. 2) and the corresponding Standard Deviations, were calculated from the remaining measurements of deflection. Fig. 6 shows the elimination of the first three measurements of deflection for the measurement between two aluminium cylinders with the same diameter ($d = 50$ μm). The first three are marked with a diamond, while the remaining 17 measurements are marked with a star. Fig. 7, left, presents Hamaker coefficients A_{12} [zJ] between two materials across the vacuum used in measurements and calculations in our models. We used [23] as a source for the Hamaker coefficients between the metals (Ag, Al, Au, Ni, Pd) and the sapphire in a vacuum. We used [24] as a source for the Hamaker coefficients of the polystyrene, SiO_2 and sapphire in a vacuum, and we used [25] as a source for the Hamaker coefficient of mica in a vacuum. Eq. 11 was used to calculate all the Hamaker coefficients Ahmadi [24] presented in Fig. 7, left.

$$A_{12} \approx \sqrt{A_{11}}\sqrt{A_{22}} \tag{11}$$

Fig. 7, right, presents the measured values of van der Waals force F_m [μN] and their Standard Deviations calculated from the measured deflections. The same Fig. 7, right, also presents the calculated van der Waals force F_c [μN] obtained from the contact model of van der Waals forces using Eq. 3, Eq. 4, Eq. 5 and Eq. 9 for control check using calculated van der Waals distance d_c [Å]. The distances at van der Waals peak d_m [Å] between different materials and geometrical appearance were determined from Eq. 3 for the sphere-sphere geometrical combination, from Eq. 4 for the sphere-surface plane geometrical combination, from Eq. 5 for two infinite perpendicular cylinders with the same radius, and from the neural network for a cylinder-sphere combination.

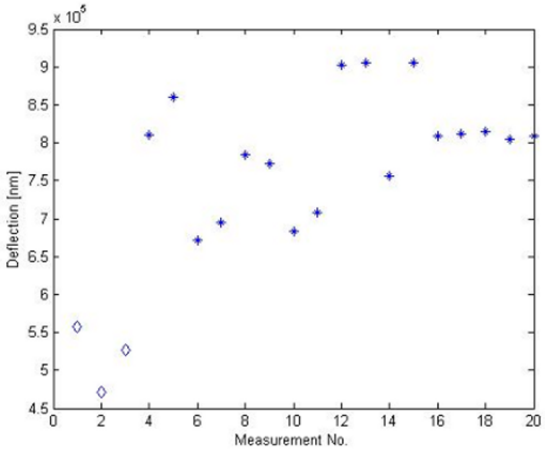

Fig. 6 Elimination of the deflection measurements that deviated significantly from the average value in contact between two aluminium cylinders, both with diameters $d = 50$ μm

Calculated distances at van der Waals peak d_c [Å] were cross-calculated with Eq. 10 from determined distances at van der Waals peak d_{12} or d_{22} or d_{11}. Both distances at van der Waals peak d_m [Å] and d_c [Å] for materials used in the experiment are presented in Fig. 8, left. The absolute value of percentage deviation $|F_d|$ [%] between measured and calculated van der Waals forces F_m and F_c were compared to validate the models for determining the van der Waals force in con

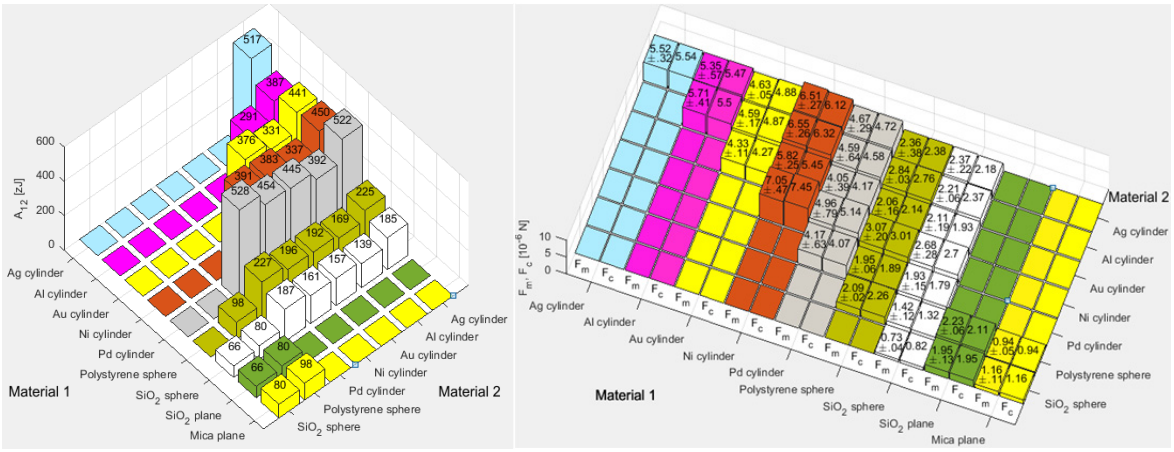

Fig. 7 Hamaker coefficients between materials across the vacuum used in calculations Measured (F_m [μN]), and calculated F_c [μN] van der Waals forces in contact between different materials used in the experiment

tact and presented in Fig. 8, right. So, for example, when material 1 is Ag and material 2 is Ag, the measured van der Waals force F_m with a value of 5.52 ± 0.32 μN was measured (see Fig. 7, right) using the method described by Eq. 2 and Fig. 3d. Then, the value $d_m = d_{11} = 6.25$ Å for the Ag-Ag combination of materials was calculated using Eq. 5 (see Fig. 8, left). The same was done for an Al-Al combination of materials with the value $d_m = d_{22} = 4.62$ Å, and an Ag-Al combination of materials with the value $d_m = d_{12} = 5.52$ Å. After that, using Eq. 10, the value $d_c = d_{12} = d_{11}/2 + d_{22}/2 = 6.25$ Å $/2 + 4.62$ Å $/2 = 5.43$ Å was calculated. The value d_c was used to obtain the calculated van der Waals force $F_c = 5.47$ μN for the case of the Ag-Al combination of materials, using Eq. 5 again (see Fig. 8, right). The values $F_c = 5.47$ μN and $F_m = 5.35 \pm 0.57$ μN for the Ag-Al combination of materials were compared, and, finally, the absolute value of percentage deviation between both values $F_d = 2.6$ % was calculated (see Fig. 8, right). With the same method, the measured and calculated values were cross calculated, and statistical validity was verified for the proposed method and model. This method used Eq. 3, Eq. 4, Eq. 5 and Eq. 9 for calculating van der Waals forces in contact.

Finally, the average values $d_c = d_{11}$ were calculated for material combinations where both materials are the same (Ag-Ag, Al-Al, Au-Au, Ni-Ni, Pd-Pd, Polystyrene-Polystyrene, SiO_2-SiO_2). By using Eq. 10, we calculated all $d_c = d_{11}$ by using all possible combinations of the $d_m = d_{12}$ determined values. For example, to calculate the average $d_c = d_{11} = 6.24$ Å (see Fig. 8, left) for the material combination of Ag-Ag, six determined values of $d_m = d_{12}$ material combinations can be used; Ag-Al ($d_m = d_{12} = 5.52$ Å), Ag-Au ($d_m = d_{12} = 6.30$ Å), Ag-Ni ($d_m = d_{12} = 5.36$ Å), Ag-Pd ($d_m = d_{12} = 6.84$ Å), Ag-Polystyrene ($d_m = d_{12} = 4.34$ Å) and Ag-SiO_2 ($d_m = d_{12} = 4.81$ Å). From the value $d_c = d_{11}$ for the material combination of Ag-Ag, obtained from the material combination of Ag-Al, we get $d_c = d_{11}$ (of Ag-Ag) $= 2\,d_m$ (of Ag-Al) – d_m (of Al-Al), as seen in Eq. 10. In this way, we obtained values $d_c = d_{11}$ for the material combination of Ag-Ag from all five remaining mate-

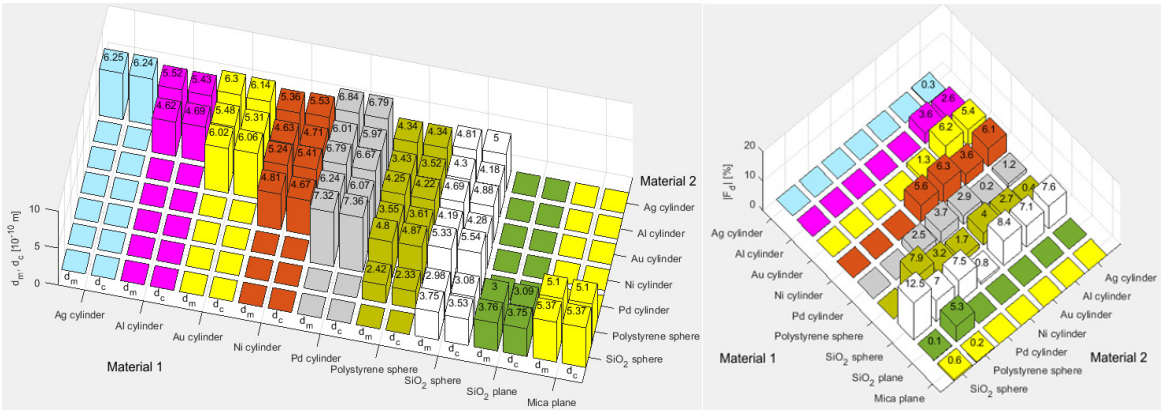

Fig. 8 Determined d_m [Å] and calculated d_c [Å] distances at van der Waals peak and for materials used in the experiment, and Absolute value of percentage deviation $|F_d|$ [%] between F_m and F_c

rial combinations (Ag-Au, Ag-Ni, Ag-Pd, Ag-Polystyrene, Ag-SiO_2). These six values $d_c = d_{11}$ were averaged to achieve a final validation of the determined and calculated value of $d_c = d_{11} = 6.24$ Å for the material combination of Ag-Ag.

3.2 Analysis of the results and discussion

The calculated van der Waals force F_c corresponded with the measured van der Waals force F_m inside the -8.4 % to 12.5 % band. The most inaccurate values are in the column called SiO_2 sphere, the highest F_d [%] gives the experimental measurements between the SiO_2 sphere and the SiO_2 sphere (12.5 %), and between the SiO_2 sphere and the Au cylinder (-8.4 %). The reason for this is that the micro-sized and nano-sized roughness of the SiO_2 spheres was "huge" in comparison with other materials. The asperities of roughness for the SiO_2 spheres were so big that the spherical geometry of the SiO_2 sphere was compromised (see Fig. 9, left). Consequently, the correct radius of the SiO_2 sphere was not determined, and this fact produced a relatively huge error in calculating the distance at van der Waals peak *d* from the measured van der Waals force. Fig. 9 shows the micro-sized and nano-sized irregularities on the surface of some of the used materials in the experiment. We tried to avoid these irregularity problems by repeating the measurements of the deflection *f* in various places. Consequently, we had to move the contact points of measurement by a few micrometres each time. These problems were the source of occasionally scattered data of deflection measurements (Fig. 6), where the first three measurements were eliminated from the set of data used for calculating the average van der Waals force and its Standard Deviation. The next reason for the mistake was, again, the radii of spheres and cylinders used in the experiment. They were determined with an accuracy of ± 1 μm, which can lead to an error in calculating the van der Waals force up to ± 4 %. Another source of errors in the model of the van der Waals force in contact could be the Hamaker coefficients used in the experiments. Different sources give different values for the Hamaker coefficients of the used materials, however, this didn't increase the relative deviation (F_d [%]), but increased the absolute error of the calculated van der Waals forces and the determined distances at van der Waals peak.

Of course, distances at van der Waals peak, determined by [7], (d_{Al}), have to be smaller than our values d_{11}, d_{12} and d_{22}, because he used the crystallographic method to determine these. Therefore, their measurements were "not spoiled" by asperities of nano-roughness and the "roughness of the crystal structure" of the materials used in the experiment. Distances at van der Waals peak determined by our method were always higher than those obtained by Alvarez (distances at van der Waals peak determined for Ag-O is $d_{Ag} = 5.2$ Å, for Al-O is $d_{Al} = 4.0$ Å, for Au-O is $d_{Au} = 4.0$ Å, for Ni-O is $d_{Ni} = 4.1$ Å, for Pd-O $d_{Pd} = 4.2$ Å and for O-O is $d_O = 3.3$ Å; O presents the oxygen probe, such as SiO_2, Al_2O_3, etc) from the source [7] just for comparison with our determined distances at van der Waals peak. The distances at van der Waals peak determined by our method were always higher than those obtained by Alvarez [7]. There is only one exception, where the distance at van der Waals peak was determined and calculated between the Ag cylinder and the SiO_2 sphere. We double checked our force measurements, but the determined values of distances at van der Waals peak were always between 4.8-4.9 Å. We believe that in [7] there is an error in obtaining the distance at van der Waals peak by using the crystallographic method for the Ag-O measurements, because the author claimed that "*Ag-O has a poorly defined peak and larger uncertainty in its position*".

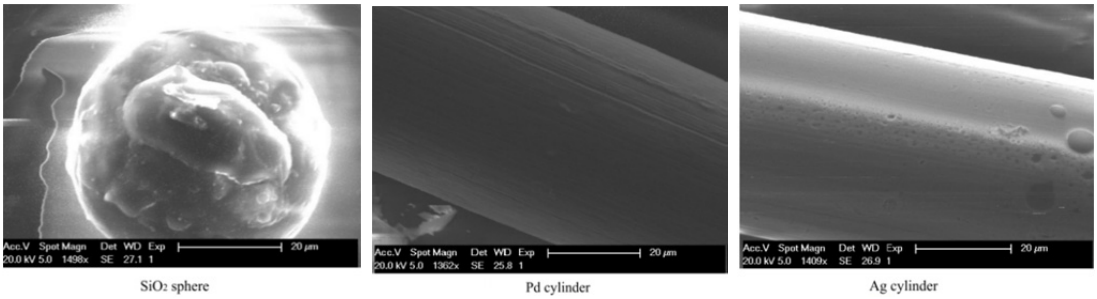

Fig. 9 SEM images of geometrical shapes and roughness of some of the materials used in the experiments

It can also be confirmed by calculating the van der Waals radius for Ag. This can be seen in [27, 28], where van der Waals radius for Ag deviates from [7]. However, other data agree on the majority of other elements of the periodic system. Young's modulus E in Eq. 2 is also an example of an error in measuring the van der Waals force in contact using the pull-off method. Young's modulus for gold varies between 79-80 GPa, which brings measurement error of up to 1 %. For the final experiment, we built a one-layer triangle structure (Fig. 10) by using many micro objects (spheres) scattered on the plane surface. By using the presented method, we were able to determine the proper size of the micro-objects from Hamaker coefficient, geometry, and distance at van der Waals peak, prior to manipulation of the objects. If the measured van der Waals force was not as expected (too small or too big), the object was not suitable to be part of the microstructure.

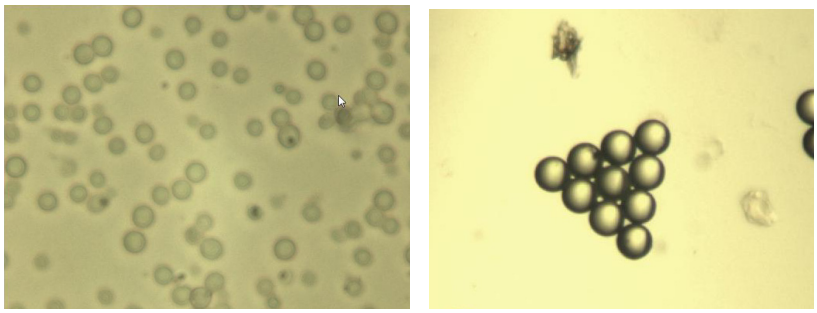

Fig. 10 Scattered micro-objects on the plane (left), and built triangle with cca. 30 μm spheres in diameter

4. Conclusion

The paper presents a method for micro/ nano 3D assembly, where visual information about the objects is not available. By knowing the material type and geometry, a micro-object's properties (e.g. size) can be determined based on van der Waals force measurement and distance at van der Waals peak determination. We present a new model for determining the distance at van der Waals peak and, consequently, measuring the van der Waals force in contact between micro-sized objects, the micro-sized objects being of different materials (metallic wires…), shapes, nano-sized roughness and crystal structure roughness. We have demonstrated experimentally that the distance at van der Waals peak determined with our pull-off method determines the sum of the van der Waals radius, the average impact of nano-sized asperities and the crystal structure roughness of the materials' contact surfaces effectively. Our model for measuring the van der Waals force in contact is more accurate than [13], and easier to use than the methods previously published in [9-12], because they used more sophisticated methods with more expensive equipment (AFM, X-ray devices). An important outcome is the experimental confirmation of Eq. 10, where, if the distances at van der Waals peak are determined between one type of material and a second type of material, we can derive the distance at van der Waals peak for a mixture of both types of material. Consequently, an accurate value of the van der Waals force can be calculated for both materials in contact. The drawback of the presented pull-off method for measuring van der Waals forces in contact is that it is highly sensitive to micro-sized irregularities, e.g. both, or even only one of the materials in contact, have micro-sized irregularities on their surface.

Acknowledgement

This research was partly funded by the Slovenian Research Agency under Grant No. P2-0123(B) Clothing Engineering and Textile Materials.

References

[1] Ngo, T.D., Kashani, A., Imbalzano, G., Nguyen, K.T.Q., Hui, D. (2018). Additive manufacturing (3D printing): A review of materials, methods, applications and challenges, *Composites Part B: Engineering,* Vol. 143, 172-196, doi: 10.1016/j.compositesb.2018.02.012.

[2] Ru, C., Luo, J., Xie, S., Sun, Y. (2014). A review of non-contact micro- and nano-printing technologies, *Journal of Micromechanics and Microengineering*, Vol. 24, No. 5, Article 053001, doi: 10.1088/0960-1317/24/5/053001.

[3] Šafarič, R., Lukman, D. (2014). One-finger gripper based on the variable van der Waals force used for a single nano/micro-sized object, *Journal of Micromechanics and Microengineering*, Vol. 24, 1-13, doi: 10.1088/0960-1317/24/8/085012.

[4] Uran, S., Šafarič, R., Bratina, B. (2017). Reliable and accurate release of micro-sized objects with a gripper that uses the capillary-force method, *Micromachines*, Vol. 8, No. 6, 182, doi: 10.3390/mi8060182.

[5] Kudryavtsev, Y.V., Gelinck, E., Fischer, H.R. (2009). Theoretical investigation of van der Waals forces between solid surfaces at nanoscales. *Surface Science*, Vol. 603, No. 16, 2580-2587, doi:10.1016/j.susc.2009.06.007.

[6] Rowland, R.S., Taylor, R. (1996). Intermolecular nonbonded contact distances in organic crystal structures: Comparison with distances expected from van der Waals radii, *The Journal of Physical Chemistry*, Vol. 100, No. 18, 7384-7391, doi: 10.1021/jp953141.

[7] Alvarez, S. (2013). A cartography of the van der Waals territories, *Dalton Transactions*, Vol. 42, 8617-8636, doi: 10.1039/c3dt50599e.

[8] Rumpf, H. (1990). *Particle Technology*, Chapman and Hall, London, UK.

[9] Rabinovich, Y.I., Adler, J.J., Ata, A., Singh, R.K., Moudgil, B.M. (2000). Adhesion between nanoscale rough surfaces I. Role of asperity geometry, *Journal of Colloid and Interface Science,* Vol. 232, No. 1, 10-16, doi:10.1006/jcis.2000.7167.

[10] Rabinovich, Y.I., Adler, J.J., Ata, A., Singh, R.K., Moudgil, B.M. (2000). Adhesion between nanoscale rough surfaces II. Measurement and comparison with theory, *Journal of Colloid and Interface Science,* Vol. 232, No. 1, 17-24, doi:10.1006/jcis.2000.7168.

[11] Katainen, J., Paajanen, M., Ahtola, E., Pore, V., Lahtinen, J. (2006). Adhesion as an interplay between particle size and surface roughness, *Journal of Colloid and Interface Science*, Vol. 304, No. 2, 524-529, doi: 10.1016/j.jcis.2006.09.015.

[12] Matope, S., van der Merwe, A.F., Nemutudi, R., Nkosi, M., Maaza, M. (2011). Micro-material handling employing E-beam generated topographies of copper and aluminium, *The South African Journal of Industrial Engineering*, Vol. 22, No. 2, 175-188, doi:10.7166/22-2-24.

[13] Matope, S., van der Merwe, A.F., Rabinovich, Y.I. (2013). Silver, copper and aluminium coatings for micro-material handling operations, *The South African Journal of Industrial Engineering*, Vol. 24, No. 2, 69-77, doi: 10.7166/24-2-554.

[14] Eichenlaub, S., Gelb, A., Beaudoin, S. (2004). Roughness models for particle adhesion, *Journal of Colloid and Interface Science,* Vol. 280, No. 2, 289-298, doi:10.1016/j.jcis.2004.08.017.

[15] Škorc, G., Šafarič, R. (2012). Adaptive positioning of MEMS production system with nano-resolution, *Intelligent Automation & Soft Computing,* Vol. 18, No. 4, 381-398, doi: 10.1080/10798587.2012.10643250.

[16] Lambert, P. (2007). *Capillary Forces in Microassembly*, Springer, Boston, USA.

[17] Kraut, B. (2003). *Strojniški priročnik*, Založba Litostroj, (in Slovene), Ljubljana, Slovenia.

[18] Parsegian, V.A. (2006). *Van der Waals Forces,* Cambridge University press, UK.

[19] Montgomery, S.W., Franchek, M.A., Goldschmidt, V.W. (2000). Analytical dispersion force calculation for nontraditional geometries, *Journal of Colloid and Interface Science*, Vol. 227, No. 2, 567-584, doi: 10.1006/jcis.2000.6919.

[20] Visser, J. (1976). Adhesion of colloidal panicles, In: Matijevic, E., Borkovec, M. (eds.), *Surface and Colloid Science*, Vol. 8, John Wiley & Sons, New York, USA, 3-84.

[21] Kirsch, V.A. (2003). Calculation of the van der Waals force between a spherical particle and an infinitive cylinder, *Advances in Colloid and Interface Science*, Vol. 104, No. 1-3, 311-324, doi: 10.1016/S0001-8686(03)00053-8.

[22] Šafarič, R., Rojko, A. (2007). *Inteligentne regulacijske tehnike v mehatroniki*, (in Slovene), Tiskarna tehniških fakultet, Maribor, Slovenia.

[23] Lipkin, D.M., Israelachvili, J.N., Clarke, D.R. (1997). Estimating the metal-ceramic van der Waals adhesion energy, *Philosophical Magazine: A*, Vol. 76, No. 4, 715-728, doi: 10.1080/01418619708214205.

[24] Ahmadi, G. London-van der Waals Force, Clarkson University, from *https://webspace.clarkson.edu/projects/crcd/public_html/me437/downloads/5_vanderWaals.pdf*, accessed January 25, 2018.

[25] Attraction – Dispersion energies (2008), from *http://soft-matter.seas.harvard.edu/index.php/Attraction_-_Dispersion_energies*, accessed January 10, 2018.

[26] Bondi, A. (1966). Van der Waals volumes and radii of metals in covalent compounds, *The Journal of Physical Chemistry*, Vol. 70, No. 9, 3006-3007, doi: 10.1021/j100881a503.

[27] Batsanov, S.S. (2001). Van der Waals radii of elements, *Inorganic Materials*, Vol. 37, No. 9, 871-885, doi: 10.1023/A:1011625728803.